

Feature Extraction Using Generalized Interpolating Wavelets

Zhuoer Shi, D. S. Zhang, H. X. Wang, D. J. Kouri, J. U. Quevedo, I. Kakadiaris,
G. H. Gunaratne, and D. K. Hoffman

Abstract— We present an improved imaging technique with a particular emphasis on mammogram enhancement. Interpolating distributed approximating functional (DAF) wavelets, visual group normalization (VGN), and nonlinear multiscale edge sharpening techniques are developed. These are formulated to normalize the wavelet coefficients, remove perceptual redundancy, as well as improve the visualization of the important diagnostic features for digital mammograms. Without prior knowledge of the “true” spatial distribution of the signal, excellent enhancement results can be obtained by the present techniques.

Index Terms— Distributed approximating functional, visual group normalization.

I. INTRODUCTION

For women 35-54, breast cancer has the highest incidence rate and is the leading cause of death. Approximately one of every eight women will develop breast cancer at some time during her life [4]. A failure to detect the early signs of breast cancer can result in a progression of the disease from the early stage, in which the cancer is confined within the breast, to later stages, in which the cancer has invaded or metastasized to other parts of the body. In late-stage cancer, treatment becomes more expensive and the patient's chances for survival are dramatically lower. The five-year survival rate for breast cancer patients decreases from approximately 96% for early stage cancers to 20% for late stage cancers that have spread to distant organs. Because survival rates are highest and recurrence and treatment costs are lowest if the cancer is detected and treated at an early stage, it is critical to diagnose breast cancer as early as possible.

The successful use of screen-film mammography in breast cancer screening is one of the major achievements for medical imaging in this century. Mammography is acknowledged to be the single most effective method of screening for breast cancer and is credited with reducing breast cancer mortality by at least 30% for women aged 40 and older. The recommendation that women aged 50 and older have regular mammograms is universally accepted on the basis that the increases in breast cancer incidence in women aged 50 and older are greater than for younger women. However, screen-film mammography has a number of limitations, a fact that has encouraged investigation of whole-breast digital mammography as a possible complement or alternative. Some successful devices include the large-area detector developed by Bennett X-ray (Copiague, NY), the slot-scanning digital mammography unit developed by Fischer Imaging (Denver, Colo), and the Senographe System developed by GE Medical Systems (Schenectady, NY), etc. Because the clinical images can be enhanced after the exam with advanced computer technology, the digital x-ray system has the potential to increase productivity by reducing the need for retakes of suspicious areas. Early trials show that digital mammography improves the spatial and contrast resolution.

Although the film (and digital) mammographic quality has increased significantly over the years, radiologists still acknowledge that mammography has “inherent limitations” [3]. The human eye can discriminate among about 20 percent of all possible shades. Most of these are those occurring in regions with the highest contrast. But the most telling information in a mammogram can occur in less-discriminated

regions of gray. That means that much of the information contained in a mammogram is never read because the human eye cannot distinguish it. As many as 10 percent of all cases of breast cancer go undetected by mammography [3]. Several studies have shown that approximately half of the undetected cancers are missed due to observational oversights by the radiologists [15]. Much of this is consequence of the fact that mammography has a much lower dynamic range than chest, bone, and gastrointestinal radiography.

The advanced breast-imaging technologies aim to improve tissue differentiation for improved determination of the detailed structure of breast lesions, as well as enhance the ease of detecting most suspicious masses, define tumor borders and structure, and thereby effectively localize lesions. The processed results are intended to improve the detection performance of the computer-aided-diagnosis (CAD) system, in terms of enhanced detection probability and decreased false detection. They can improve the speed and accuracy of mammograms by finding features too subtle for the human eye to see. Such technology is of great importance for telemedicine applications. The use of telecommunications and information technology to deliver clinical health-care services, has become a fixture in some rural hospitals in the United States. Using real-time teleconferencing equipment and the Internet, telemedicine allows rapid communication between investigators, speeds the translation of articles, and improves information access and education in developing countries. Telemedicine already is used in a variety of medical specialties, including telepsychiatry, teleophthalmology, telerehabilitation, and teleradiology. Teleradiology, the most practiced specialty in telemedicine has the potential allowing researchers from remote locations to examine and manipulate high-resolution, filmless “electronic slides” of cells and tumors.

We propose a new multiresolution mammogram enhancement technique in this paper. Sinc distributed approximating functionals (Sinc-DAFs), designed as a set of envelope-modulated interpolants [21, 22], are utilized to generate a new class of interpolating wavelets. Such DAFs and DAF-wavelets are smooth and decaying in both time and frequency domains and have been used for numerically solving a variety of linear and nonlinear partial differential equations (PDEs) with extremely high accuracy and computational efficiency. The attractive property of the interpolating wavelets is that the discrete subband decomposition coefficients are obtained from linear combinations of discrete samples rather than from traditional inner product integrals [12]. Without any pre-conditioning or post-conditioning processes for accurate wavelet analysis, the wavelet coefficients are implemented using a fast-parallel computational scheme. This is a specifically matched design for the mammographic solution involving huge data sets and high resolution (normally hundreds of megabytes for a single digital picture).

To obtain excellent enhancement quality of a digital mammogram, subband filter response and human visual sensitivity are utilized to implement the *visual group normalization* (VGN) technique, which is used to re-scale the decomposition coefficients for the next-step of perceptual adapted reconstruction. Carefully-designed nonlinear contrast stretch and enhancement functionals are constructed and employed for a multiscale gradient transformation to obtain the feature-preserved solution, which enables us to obtain accurate space-localization of the important diagnosis characteristics. The combined techniques greatly improve the visualization of low-contrast components of a mammogram and efficiently deal with its huge amount of data, complicated space-frequency distribution and complex perceptual dependent characteristics. We have successfully launched the associated software analysis system, named—DAF Sparkle™, which provides an interactive system that can revolutionize the mammographic approach to breast cancer. Given the importance of early detection, it is believed that the present technology represents a significant contribution to screening and digital mammography.

This work was supported by the National Science Foundation under Grant CHE-9700297, the R. A. Welch Foundation under Grant E-0608, and the Department of Energy under Contract 2-7405-ENG82.

Z. Shi, D. S. Zhang, H. X. Wang, D. J. Kouri, and G. H. Gunaratne are with the Department of Physics and Chemistry, University of Houston, Houston, TX 77204. (e-mail: zshi@bayou.uh.edu, dszhang@bayou.uh.edu, hxwang@bayou.uh.edu, kouri@uh.edu, gemu@uh.edu).

J. U. Quevedo and I. Kakadiaris are with the Department of Computer Science, University of Houston, Houston, TX 77204. (e-mail: jquevedo@cs.uh.edu, ioannisk@uh.edu).

D. K. Hoffman is with the Department of Chemistry and Ames Laboratory, Iowa State University, Ames, IA 50011. (e-mail: hoffman@ameslab.gov).

II. DESIGN OF GENERALIZED INTERPOLATING WAVELETS

To enable the multiscale processing of mammography, we introduce an interesting construction for interpolating wavelets. The interpolating aspect of the wavelet design comes from the π band-limited Sinc function

$$\phi(x) = \sin(\pi x)/(\pi x) \in C^\infty \quad (1)$$

in *Paley-Wiener* space. Every π band-limited function $f \in L^2(\mathbb{R})$ can be exactly reconstructed by the expression

$$f(x) = \sum_k f(k) \frac{\sin \pi(x-k)}{\pi(x-k)} \quad (2)$$

If we regard the Sinc as a scaling function, then the associated wavelet function—*Sinclet*, is defined as (see Figure 1)

$$\psi(x) = \frac{\sin \pi(2x-1) - \sin \pi(x-1/2)}{\pi(x-1/2)} \quad (3)$$

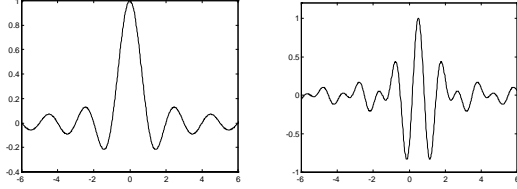


Figure 1. Band-limited interpolating wavelets. (a) *Sinc* function. (b) *Sinclet* wavelet.

The scaling Sinc function is, of course, the well-known ideal low-pass filter, which possesses the filter response

$$H(\omega) = \begin{cases} 1, & |\omega| \leq \pi/2 \\ 0, & \pi/2 < |\omega| \leq \pi \end{cases} \quad (4)$$

Its impulse response can be described as

$$h[k] = \frac{1}{2\pi} \int_{-\pi/2}^{\pi/2} e^{jk\omega} d\omega = \frac{\sin(k\pi/2)}{k\pi} \quad (5)$$

The so-called half-band filter only possesses non-zero impulses at odd integer samples, $h(2k+1)$, while at even integers, $h[2k] = 0$, except for $k = 0$.

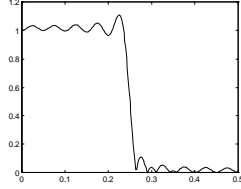


Figure 2. Gibbs overshoot of Sinc FIR implementation.

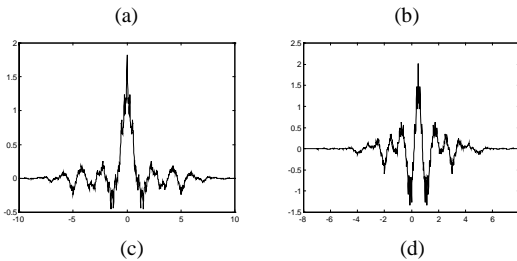
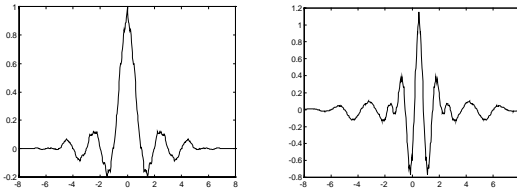


Figure 3. Sinc cutoff wavelets (filter $h(k)$, $k = -9, 9$).

(a) Scaling. (b) Wavelet. (c) Dual scaling. (d) Dual wavelet.

However, as is well known, this ideal low-pass filter can not be implemented physically. Because the digital filter is an IIR (infinite impulse response) solution, its digital cutoff FIR (finite impulse response) implementation introduces the Gibbs phenomenon (overshoot effect) in Fourier space, which degrades the frequency resolution (as shown in Figure 2). The compactly supported Sinc scaling function and wavelet, as well as their biorthogonal dual scaling function and wavelet, are shown in

Figure 3. We observe that the cutoff wavelet construction has decreased regularity, which is manifested by a fractal-like behavior, which implies poor time localization.

Because the ideal Sinc wavelet can not be implemented “ideally” by FIR (finite impulse response) filters, we (and others) introduce a windowed weighting technique to eliminate the cutoff singularity and improve the time-frequency localization of the wavelets. A symmetric Sinc interpolating shell is defined by

$$P(x) = \frac{\sin(\pi x/2)}{\pi x} \quad (6)$$

Multiplying this shell with a smooth window which vanishes gradually, leads to the construction of regular wavelets and equivalent subband filters (as shown in Figure 4 and Figure 5). One possible design is to employ the Sinc distributed approximating functionals (DAF) as the scaling function,

$$\phi_\sigma(x) = W_\sigma(x)P(x) = W_\sigma(x) \frac{\sin(\pi x/2)}{\pi x} \quad (7)$$

where $W_\sigma(x)$ is a Gaussian window function,

$$W_\sigma(x) = e^{-x^2/2\sigma^2}, \quad (8)$$

and σ is a window width parameter.

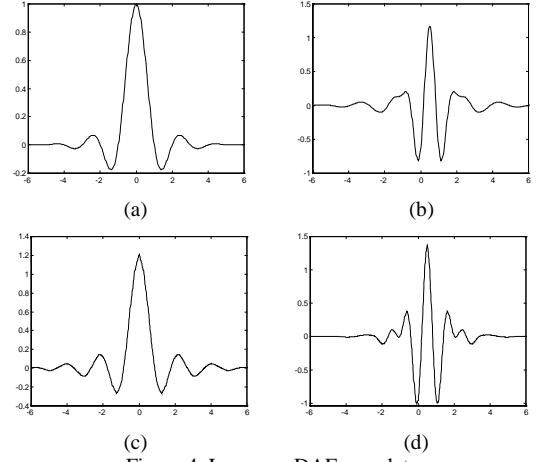


Figure 4. Lagrange DAF wavelets.

(a) Scaling. (b) Wavelet. (c) Dual scaling. (d) Dual wavelet.

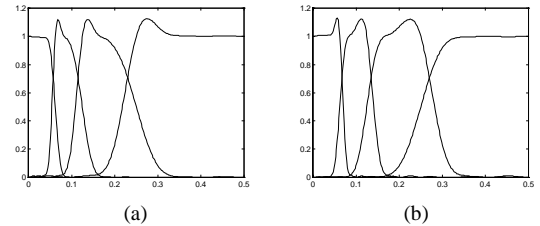


Figure 5. Frequency response of equivalent filters. (a) Decomposition. (b) Reconstruction.

Because the Gaussian window satisfies the minimum frame bound condition in quantum physics, it will improve the time-frequency resolution of the derived wavelet. Such a DAF scaling function has been successfully applied as an efficient and powerful grid method for quantum dynamical propagation and other physics applications [21]. Examples include simulations of 3D reactive quantum scattering, the Kuramoto-Sivashinsky equations describing flame-front pattern dynamics for a circular domain burner, the sine-Gordon equation near homoclinic orbits, and a 2D Navier-Stokes equation with non-periodic boundary conditions [22, 55, 56]. The Gaussian design efficiently smoothes out the fractal oscillations, which plague most conventional wavelet bases. The interpolation relation

$$\phi(k) = \begin{cases} 1, & k = 0, \quad k \in \mathbb{Z} \\ 0, & k \neq 0 \end{cases} \quad (9)$$

and the self-induced two-scale relation

$$\phi(x) = \sum_k \phi(k/2)\phi(2x-k) \quad (10)$$

lead to the filter impulse response

$$h(k) = \frac{1}{2} \phi_\sigma \left(\frac{k}{2} \right), \quad k = -2M+1, 2M-1 \quad (11)$$

The Gaussian can be estimated by a B-spline function [48] with order D , $\beta_D(x)$, according to

$$\beta_D(x) \equiv \sqrt{\frac{6}{\pi(D+1)}} \exp\left(\frac{-6x^2}{D+1}\right). \quad (12)$$

Because such an interpolating wavelet-based multiresolution space is identical to the discrete sampling space, the subband decomposition is implemented by linear interpolation rather than the conventional convolution. This enables a massively parallel calculation strategy for the huge data sets encountered in mammography. Furthermore, the time-frequency optimization of the DAF wavelet enables stable, localized feature extraction from the transform coefficients. Mathematically, interpolating wavelets can be formulated in a lifting biorthogonal setting [45], an extension of the auto-correlation shell analysis [37], halfband filters [1], a kind of piecewise polynomial [18], and a special case of the Neville filters [26]. Generally speaking, the interpolating wavelet theory is closely related to the finite element technique in the numerical solution of partial differential equations, the subdivision scheme for interpolation, multi-grid generation and surface fitting techniques.

III. VISUAL GROUP NORMALIZATION

A. Magnitude Normalization

On each decomposition level, 2D wavelet coefficients of mammography are divided into four sub-blocks, LL , HL , LH , and HH . As usual, L and H represent the low-pass and high-pass subband filtering results, respectively. The detailed sub-blocks HL , LH and HH represent the multiscale difference operation in three different decomposition orientations, horizontal, vertical, and diagonal, respectively. At each level of analysis, the bandwidth of the equivalent subband filters decreases by a factor of two.

Wavelet coefficients can be regarded as the output of the signal passing through equivalent decomposition filters (EDF). The responses of the EDF are the combination of several recurrent subband filters at different stages [52]. The EDF amplitudes of various sub-blocks differ greatly. Thus, the magnitude of the decomposition coefficients in each of the sub-blocks cannot exactly reproduce the actual strength of the signal components. To adjust the magnitude of the response in each block, the decomposition coefficients $C_{j,m}(k)$ in block (j,m) should be multiplied with a magnitude scaling factor, $\lambda_{j,m}$, to obtain an adjusted magnitude representation. Here j represents the decomposition layer, and m denotes the different orientation block (LL , LH , HL or HH). The normalizing factor is defined as the reciprocal of the maximum magnitude of the frequency response of the equivalent wavelet decomposition filter on node (j,m)

$$\lambda_{j,m} = \frac{1}{\sup_{\omega \in \Omega} \{|LC_{j,m}(\omega)|\}}, \quad \Omega = [0, 2\pi] \quad (13)$$

Thus, the magnitude normalized coefficients, $NC_{j,m}(k)$, are defined as

$$NC_{j,m}(k) = \lambda_{j,m} C_{j,m}(k). \quad (14)$$

This idea was recently extended to *group normalization* (GN) theory and was shown to yield the optimal performance for signal detection [41, 42]. The magnitude normalization unifies the coefficient strength in each of the subblocks. However, an image is a signal source processing an additional perceptual property. Coefficients with equal magnitude (after the magnitude normalization) in different frequency channels result in greatly different visual gain (sensitivity) for human eyes. Additional alterations of the coefficients are required for perceptual image processing.

B. Perceptual Lossless Normalization

The reconstruction visibility of wavelet transform coefficients depends upon the display visual resolution [54] in pixel/degree. Given a viewing distance V in inches and a display resolution d in pixel/inch, the effective display visual resolution (DVR) R in pixel/degree of visual angle is

$$R = dV \tan(\pi/180) \approx dV/57.3 \quad (15)$$

The visual resolution is the viewing distance in pixels (dV) divided by 57.3. As mentioned above, when the decomposition layer increases, the bandwidth of the equivalent subband filters decreases by a factor of two. Thus the frequency resolution doubles. Correspondingly, the space (time

resolution (display resolution) decreases by a factor of two. A sub-block of wavelet coefficients corresponds to a spatial frequency band. For a display resolution of R pixel/degree, the spatial frequency f of level j is

$$f = 2^j R \quad (16)$$

For a Y -channel gray-scale mammogram image, the just-noticeable quantization threshold of Y is generally different at each spatial frequency. The contrast sensitivity declines when the spatial frequency increases (the size of the stimuli decreases). This fact is used to construct the ‘‘perceptual lossless’’ response magnitude for normalization in subblock (j,m) according to the visual response.

For images based on the human vision system (HVS), using a just-noticeable distortion profile, we can efficiently remove the visual redundancy from decomposition coefficients and normalize them with respect to the standard of perceptual importance. A simple mathematical model for perception efficiency, based on the amplitude nonlinearity in different frequency bands, has been presented in [54], which can be used to construct the ‘‘perceptual lossless’’ response magnitude $Y_{j,m}$ for normalizing visual response in different luminance/chrominance spaces. We extend the definition to luminance/chrominance modes by requiring

$$Y_{j,m} = a10 \left(\log \frac{2^j f_0 d_m}{R} \right)^k \quad (17)$$

where a defines the minimum threshold, k is a constant, R is the Display Visual Resolution (DVR), f_0 is the spatial frequency, and d_m is the directional response factor for each subblock.

The parameters d_{LL} , and d_{HH} represent the thresholds for orientations LL and HL as frequency shifts relative to the threshold for orientations LH and HL . From the nature of dyadic wavelets, the orientation LL possesses a spectrum that is approximately a factor of two lower in spatial frequency than orientation LH or HL . This would suggest a factor of $d_{LL}=2$. However, in a vision system response mechanism, at orientation LL the signal energy is spread over all matrix elements, which implies less visual efficiency than when the energy is concentrated over a narrow range, as is the case for the spectra of orientation HL or LH . Thus, the threshold should be increased, which can be achieved by a slight reduction in f_0 . The final value for d_{LL} employed is therefore less than 2.

For orientation HH , similar effects exist. First, the Cartesian splitting of the spectrum makes the spatial frequency of orientation HH about $\sqrt{2}$ higher than that of the orientations HL , and LH . Thus d_{HH} can be taken as $d_{HH}=2^{1/2}$. As we mentioned previously, the spectrum along orientation HH is spread over two orthogonal orientations (45° and 135°), which should result in a log threshold increase of about $2^{1/4}$ (a shift of $2^{-1/4}$) or a total threshold factor of $d_{HH}=2^{3/4}=0.59$. Finally, the well-known oblique effect will cause a small amount of threshold elevation.

C. Visual Sensitivity Normalization

Visual sensitivity is defined as the inverse of the contrast to produce a threshold response [26],

$$S = 1/C, \quad (18)$$

where C is generally referred to simply as the threshold. The Michelson definition of contrast,

$$C = (L_{max} - L_{mean})/L_{mean} \quad (19)$$

is used, where L_{max} and L_{mean} refer to the maximum and mean luminances of the waveform in a luminance channel. Sensitivity can be thought of as a gain, although various nonlinearities of the visual system require caution in the use of this analogy. The variations in sensitivity as a function of light level are primarily due to the light-adaptive properties of the retina and are referred to as the *amplitude nonlinearity* of the HVS. The variations as a function of spatial frequency are due to the optics of the eye combined with the neural circuitry; these combined effects are referred to as the *contrast sensitivity function* (CSF). Finally, the variations in sensitivity as a function of signal content, referred to as *masking*, are due to the post-receptor neural circuitry.

Combining the perceptual lossless normalization, the visual sensitivity normalization and the magnitude normalized factor $\lambda_{j,m}$, we obtain the perceptual lossless quantization matrix $Q_{j,m}$

$$Q_{j,m} = 2CY_{j,m}/\lambda_{j,m} \quad (20)$$

This treatment provides a simple human-vision-based normalization technique for the restoration of the most important perceptual information in a mammogram image. We call the combination of the above-mentioned three normalizations the *Visual Group Normalization* (VGN) of wavelet transform coefficients.

Such perception-based signal processing has the potential of overcoming the limits of the traditional Shannon Rate-Distortion (R-D)

theory for perception-dependent information, such as images and acoustic signals. Previously, Ramchandran, Vetterli, Xiong, Herley, Asai, and Orchard have utilized a rate-distortion compromise for image compression implementation [20, 34, 58]. Our recently derived Visual Group Normalization (VGN) technique [44] can likely be used with the rate-distortion compromise to generate a so-called Visual Rate-Distortion (VR-D) theory to improve image processing further.

IV. IMAGE PROCESSING TECHNIQUES

A. Softer Logic Masking

The main objective of wavelet signal filtering is to preserve important signal components and efficiently reduce noise components. After visual group normalization processing, coefficients have been normalized according to human visual sensitivity. An additional filtering algorithm is required for de-noising and removing perceptual redundancy. *Hard logic masking* is the commonly used nonlinear processing technique. It is similar to a bias estimated *dead-zone limiter*. Jain [23] has shown that a nonlinear dead-zone limiter, $\eta(y)$, can improve the SNR for weak signal detection. It can be expressed as

$$\eta(y) = \text{sgn}(y) \left(|y| - \delta \right)_+^\beta, -1 \leq \beta \leq 1 \quad (21)$$

where δ is a threshold value, and y is the measurable value of the coefficient. Donoho shows that the $\beta=1$ case of the above expression is a near optimal estimator for adaptive NMR data smoothing and de-noising [11]. Independently, we utilized the hard logic masking to extract efficiently a target from formidable background noise in a previous work [41, 42].

Various threshold cutoffs of multi-band expansion coefficients in hard logic masking methods are very similar to the cutoff of an FFT expansion. Thus, the Gibbs oscillations associated with the FFT will also occur in the wavelet transform using a hard logic masking. Although hard logic masking methods with appropriate threshold values do not seriously change the magnitude of a signal after reconstruction, they can cause considerable edge distortions in a signal due to the interference of additional high frequency components induced by the cutoff. The higher the threshold value, the larger the Gibbs oscillations will be.

Edges are especially important for feature preservation and precise localization for images and biomedical signals. We here present a Softer Logic Masking (SLM) method. In our SLM approach, a smooth transition band near each masking threshold is introduced so that any decomposition coefficients that are smaller than the threshold value, will be *reduced gradually* to zero rather than be *set* to zero. This treatment efficiently suppresses Gibbs oscillations and preserves signal edges, and consequently improves the quality of the reconstructed signal. Our SLM method can be expressed as

$$\hat{C}_{j,m}(k) = \text{sgn}(C_{j,m}(k)) (|C_{j,m}(k) - \delta|)_+^\beta \text{SOFT}(\overline{NC_{j,m}(k)}) \quad (22)$$

where the $\hat{C}_{j,m}(k)$ are the decomposition coefficients to be retained in the reconstruction and the quantity $\overline{NC_{j,m}(k)}$ is defined as

$$\overline{NC_{j,m}(k)} = \frac{|NC_{j,m}(k)|}{\max_{(j,m) \in T_{\text{opt}}} \{|NC_{j,m}(k)|\}} \quad (23)$$

The softer logic mapping, $\text{SOFT}: [0,1] \rightarrow [0,1]$, is a non-linear monotonically increasing sigmoid functional. A comparison of the hard and softer logic masking functionals is depicted in Figure 6.

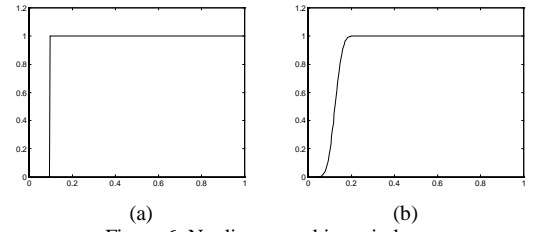
The softer logic functional can also be taken in as the alternate form

$$\hat{C}_{j,m}(k) = C_{j,m}(k) \text{SOFT} \left(\frac{NC_{j,m}(k) - \zeta}{1 - \zeta} \right), \quad (24)$$

where ζ is a normalized adaptive threshold. For an unknown noise level, an approximation to ζ is given as

$$\zeta = \gamma_{\text{upper}} \hat{\sigma} \sqrt{2 \log N / N}, \quad (25)$$

where $\hat{\sigma}$ is a scaling factor and can be chosen as $\hat{\sigma} = 1/1.349$. The quantity γ_{upper} is an upper frame bound of the wavelet packet transform, i.e., the upper bound singular value of the wavelet decomposition matrix. Using arguments similar to those given by Donoho [11], one can show that the above Softer Logic Masking reconstruction is a near optimal approximation in the min-max error sense.



(a) Hard logic nonlinearity. (b) Softer logic nonlinearity.

B. Device Adapted Enhancement

The basic idea is to use gradient operators to shape flat image data so that a desired portion of the image is projected onto a screen. Using visual normalization and softer-logic thresholding, one can efficiently remove the visual redundancy and noisy components from the decomposition coefficients.

For grayscale image contrast stretching, the objective is to improve the perception capability for image components to which the human visual system is initially insensitive, but which are important for diagnosis. In other words, mammogram enhancement aims to increase the cancer detection probability and precision. We first appropriately normalize the decomposition coefficients according to the length scale of the display device so that they fall within the interval of the device frame. Assume that the image coefficients have already been properly scaled by visual group normalization so that the amplitude value $NC_{j,m}(k)$ falls into the dynamic range of the display device:

$$d_{\min} \leq NC_{j,m}(k) \leq d_{\max} \quad (26)$$

Without loss of generality, we consider the normalized gradient magnitude,

$$U_{j,m}(k) = NC_{j,m}(k) / (d_{\max} - d_{\min}). \quad (27)$$

Wavelet multiresolution analysis provides a natural characterization for multiscale image edges, and these can be easily extracted by various differentiations. This idea was extended by Laine et al [28] to develop directional edge parameters based on a subspace energy measurement. An enhancement scheme based on complex Daubechies wavelets was proposed by Gagnon et al. [16]. These authors made use of the difference between the real and imaginary parts of the wavelet coefficients. One way or another, adjusted wavelet transforms should be designed to achieve the desired edge enhancement.

Our starting point is taken to be the magnitude-normalized or visual group-normalized wavelet subband coefficients $NC_{j,m}(k)$ [41, 42]. We define an enhancement functional $E_{j,m}$

$$E_{j,m} = \alpha_{j,m} + \beta_{j,m} \Delta, \quad (28)$$

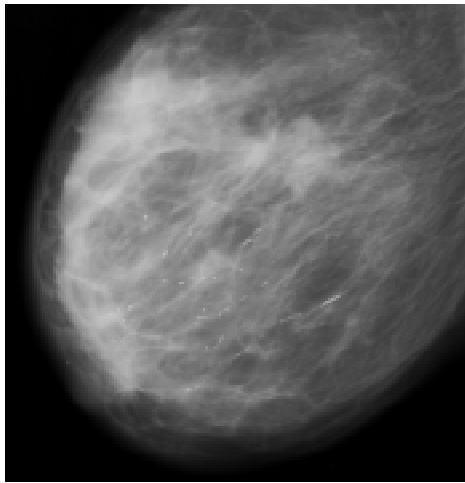
where Δ is the Laplacian and $-1 \leq \alpha_{j,m}, \beta_{j,m} \leq 1$. The coefficients $\alpha_{j,m}, \beta_{j,m}$ can be easily chosen so that desired image features are emphasized. In particular we can emphasize an image edge of selected grain size. We note that a slight modification of $\alpha_{j,m}$ and $\beta_{j,m}$ can result in orientation-selected image enhancement. A detailed discussion of this matter will be presented elsewhere. An overall re-normalization is carried out after image reconstruction to preserve the energy of the original image. We call this procedure enhancement normalization. Contrast stretching is another efficient method for feature selective image display. Nonlinear stretching has been used by many authors [10, 17, 27, 28, 46]. Lu and coworkers [29] have recently designed a hyperbolic function

$$g(k) = [\tanh(ak-b) + \tanh(b)] / [\tanh(a-b) + \tanh(b)] \quad (29)$$

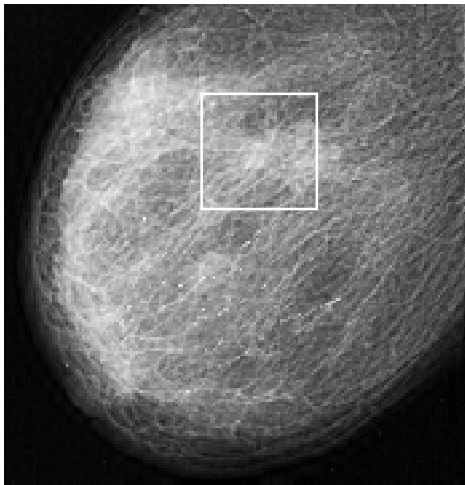
for wavelet multiscale gradient transformation. Their method works well for lunar images. The basic idea is to use gradient operators to shape a flat image so that a desired portion of the image is projected into a screen window. The two methods are combined for mammography enhancement.

V. ENHANCEMENT RESULT

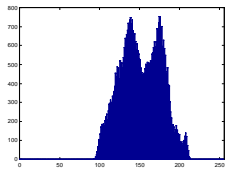
Detecting and diagnosing breast cancer is a complex clinical problem. The combination of viewing a large number of cases (99.5% of which are expected to be normal), radiologist fatigue (and the resultant observational oversights), the complex image structure of the breast on a mammogram, and the subtle nature of certain observational characteristics of the disease may result in false negative mammographic readings. The CAD system should aim to reduce both false negative and false positive mammogram readings made by the radiologist.



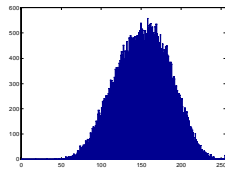
(a)



(b)



(c)

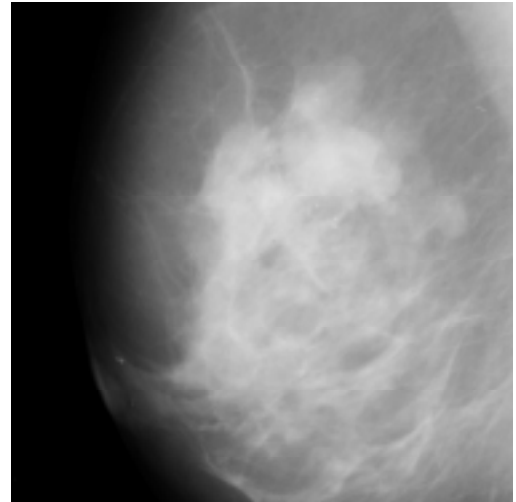


(d)

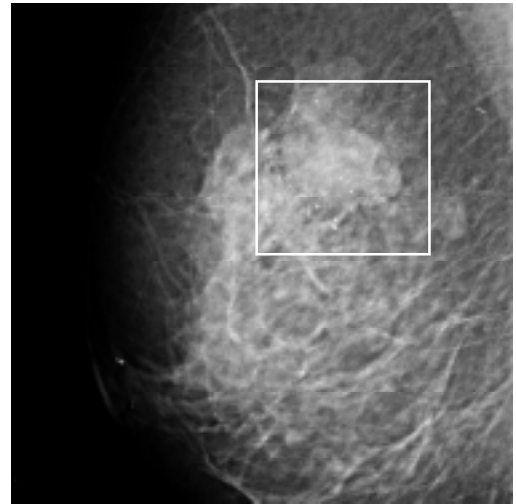
Figure 7. Spiculated mass extraction. (a) Original mammogram. (b) Our enhancement. (c) Original histogram. (d) Enhanced histogram.

Mammograms are complex in appearance and signs of early disease are often small and/or subtle. Digital mammogram image enhancement is potentially important for aiding radiologists in the development of an automatically detecting expert system. An example digitized (i.e. scanned) image mammogram is shown in Figure 7(a) and it is compared with the results of our digital enhancement technique Figure 7(b). The enhanced image shows the various “organ components” of the breast, the fibrous component of the breast, the glandular and ductal structures in the breast. The original image [59] has been chopped to a 768×800 size. Making use solely of the data in Figure 7(a), Figure 7(b) shows a significant improvement in both edge representation and image contrast resulting from DAF-wavelet-based visual group normalization (VGN) and non-linear enhancement techniques. In particular, the domain and internal tissue structure of spiculated masses (pathognomonic of breast cancer) are clearly displayed. Another test mammogram, chopped at 500×500, is shown in Figure 8(a). Our result (as shown in Figure 8(b)) is characterized by high-quality image enhancement and good signal averaging over low contrast regions with minimal resolution degradation of image details. It is possible to identify subtle pattern abnormalities of microcalcification and of an ill-defined lesion on the enhanced mammogram. The original and enhanced histograms in the marked region-of-interest (ROI) are shown in

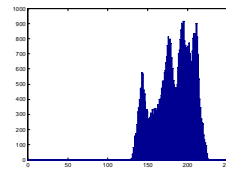
Figure 7(c), Figure 8(c), Figure 7(d) and Figure 8(d), respectively. It is easy to see that the enhanced results possess a wider dynamic gray-scale range than the originals. If it is possible to identify the portions of the histogram due to the appearance of specific types of lesions (benign or malignant) this could provide a possible automatic diagnostic tool. It is evident that our technique can make it easier to detect regions of interest (ROI) associated with cancer on a mammogram and thereby increase the percentage of cancers that are detected at the earliest possible stage, when treatment is relatively simple and the chance of a cure is greatest. The interactive “DAF Sparkle” CAD system based on our proposed technique is shown in Figure 9 which is operated on Windows NT/9X platform. A UNIX version is under development.



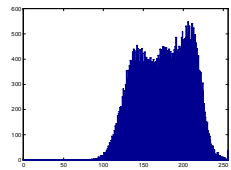
(a)



(b)



(c)



(d)

Figure 8. Microcalcification and ill-defined mass detection. (a) Original mammogram. (b) Our result. (c) Original histogram. (d) Enhanced histogram.

VI. CONCLUSION

By the end of the decade, approximately 1.8 million U.S. women will have been diagnosed with invasive breast cancer. In the U.S., approximately 180,200 new cases of invasive breast cancer are expected to

be diagnosed and nearly 43,900 women are expected to die from the disease each year. Although the healthcare facilities should expect to take a multi-year, phased approach to becoming totally filmless (a transition that requires a digital image archiving system, networking of the devices within Radiology departments, and then integrating Radiology into a hospital information system), digital mammographic processing should ultimately become the mainstream modality. Developing digital enhancement techniques to improve the visualization and interpretation of the mammography is of great importance. It can assist radiologists by minimizing the possibility of false negative and false positive readings during their view of mammograms.

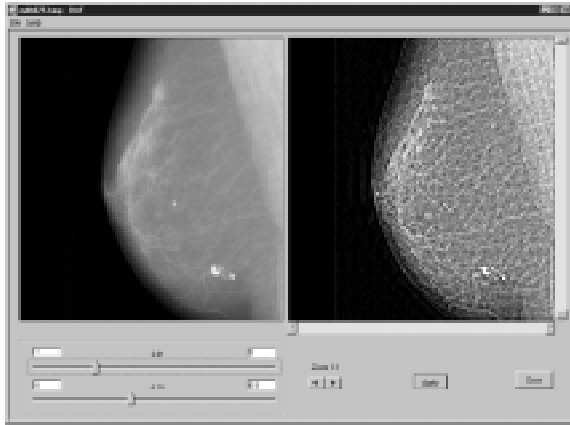


Figure 9. DAF Sparkle™ mammography analysis system.

The components of a DAF-wavelet-based image processing and enhancement approach are developed and presented in this paper. The technique integrates the construction of generalized interpolating wavelets, visual group normalization processing, series of nonlinear masking and enhancement methods that improve the mammographic imaging performance for earlier detection of cancer and malignant tumors. It increases the spatio-temporal resolution of such biomedical images and enhances the visualization of the perceptually less-sensitive components that are nevertheless very important for diagnosis, as well as reduces the distortion and blur. Different image processing (distortion suppression, enhancement, and edge sharpening) are integrated in an interactive system that can be varied by adjusting several image control parameters. The technique is capable of the speed, accuracy and image clarity required to further improve breast cancer care with high detection quantum efficiency (DQE), while still requiring and low dose X-rays. The essential capabilities required of any CAD method include high resolution, capability to delineate fine spiculations and microcalcifications, high contrast which allows visualization of subtle differences among soft-tissue densities, improved visualization of dense tissue, and ability to image of breasts of different sizes.

REFERENCES

[1] R. Ansari, C. Guillemot, and J. F. Kaiser, "Wavelet construction using Lagrange halfband filters," *IEEE Transactions on Circuits and Systems*, vol.38, no.9, pp.1116-1118, 1991.

[2] R. Baraniuk, D. Jones, "Signal-dependent time-frequency analysis using a radially Gaussian kernel," *Signal Processing*, Vol.32, pp.263-284, 1993.

[3] R. Bird, T. Wallace, B. Yankaskas, "Analysis of cancers missed at screening mammography," *Radiology*, Vol.184, pp.613-617, 1992.

[4] Breast Cancer Facts and Figures, American Cancer Society, 1997.

[5] C. M. Brislawn, "Preservation of subband symmetry in multirate signal coding," *IEEE Transactions on Signal Processing*, vol.43, no.12, pp.3046-3050, 1995.

[6] C. K. Chui, *An Introduction to Wavelets*, Academic Press, New York, 1992.

[7] A. Cohen, I. Daubechies, and J.C. Feauveau, "Biorthogonal bases of compactly supported wavelets," *Communications of Pure and Applied Mathematics*, vol. 45, pp. 485--560, 1992.

[8] I. Daubechies, "Orthonormal bases of compactly supported wavelets", *Communications of Pure and Applied Mathematics*, vol.41, no.11, pp.909-996, 1988.

[9] G. Deslauriers, S. Dubuc, "Symmetric iterative interpolation processes," *Constructive Approximations*, vol. 5, pp.49-68, 1989.

[10] A. P. Dhawan and E. Le Royer, "Mammographic feature enhancement by computerized image processing," *Computer Methods and Programs in Biomedicine*, vol. 27, no. 1, pp. 23-35, 1988.

[11] D. L. Donoho, "De-noising by soft-threshold," *IEEE Transactions on Information Theory*, vol. 41, no.3, pp. 613-627, 1995.

[12] D. L. Donoho, "Interpolating wavelet transform," Preprint, Stanford Univ., 1992.

[13] S. Dubuc, "Interpolation through an iterative scheme", *Journal of Mathematical Analysis and Applications*, vol.114, pp.185-204, 1986.

[14] S. A. Feig, M. J. Yaffe, Seminars in Ultrasound, CT, and MRI, Vol.17, No.5, pp.423-443, 1996.

[15] S. A. Feig, M. J. Yaffe, "Digital mammography," *Radiographics*, Vol. 18, pp. 893-901, August 1998.

[16] L. Gagnon, J. M. Lina, and B. Goulard, "Sharpening enhancement of digitized mammograms with complex symmetric Daubechies wavelets," preprint.

[17] R. Gordon and R.M. Rangayan, "Feature enhancement of film mammograms using fixed and adaptive neighborhoods," *Applied Optics*, vol. 23, no. 4, pp. 560-564, Feb. 1984.

[18] A. Harten, "Multiresolution representation of data: a general framework," *SIAM Journal of Numerical Analysis*, vol.33, no.3, pp.1205-1256, 1996.

[19] C. Herley, M. Vetterli, "Orthogonal time-varying filter banks and wavelet packets," *IEEE Transactions on Signal Processing*, Vol. 42, No. 10, pp.2650-2663, October 1994.

[20] C. Herley, Z. Xiong, K. Ramchandran and M. T. Orchard, "Joint space-frequency segmentation using balanced wavelet packets trees for least-cost image representation," *IEEE Transactions on Image Processing*, vol. 6, pp. 1213-1230, September 1997.

[21] D. K. Hoffman, N. Nayar, O. A. Sharafeddin, and D. J. Kouri, "Analytic banded approximation for the discretized free propagator," *Journal of Physical Chemistry*, vol.95, no.21, pp.8299-8305, 1991.

[22] D. K. Hoffman, G. W. Wei, D. S. Zhang, and D. J. Kouri, "Shannon-Gabor wavelet distributed approximating functional," *Chemical Physics Letters*, Vol. 287, pp. 119-124, 1998.

[23] L. C. Jain, N. M. Blachman, and P. M. Chapell, "Interference suppression by biased nonlinearities," *IEEE Transactions on Information Theory*, vol.41, no.2, pp.496-507, 1995.

[24] N. Jayant, J. Johnston, and R. Safranek, "Signal compression based on models of human perception", *Proceedings IEEE*, vol.81, no.10, pp.1385-1422, 1993.

[25] J. Kovacevic, and M. Vetterli, "Perfect reconstruction filter banks with rational sampling factors," *IEEE Transactions on Signal Processing*, Vol. 41, No. 6, pp.2047-2066, June 1993.

[26] J. Kovacevic, W. Swelden, "Wavelet families of increasing order in arbitrary dimensions," Submitted to *IEEE Transactions on Image Processing*, 1997.

[27] S. Lai, X. Li, and W. F. Bischof, "On techniques for detecting circumscribed masses in mammograms," *IEEE Transactions on Medical Imaging*, vol. 8, no. 4, pp. 377-386, 1989.

[28] A. F. Laine, S. Schuler, J. Fan and W. Huda, "Mammographic feature enhancement by multiscale analysis," *IEEE Transactions on Medical Imaging*, vol.13, pp.725-740, 1994.

[29] J. Lu, D. M. Healy Jr. and J. B. Weaver, "Contrast Enhancement of Medical Images Using Multiscale Edge Representation", *SPIE*, vol. 2242, *Wavelet Applications*, pp. 711-719, 1994.

[30] S. Mallat, "A theory for multiresolution signal decomposition: the wavelet representation," *IEEE Transactions on Pattern Analysis and Machine Intelligence*, Vol.11, No.7, pp.674-693, July 1989.

[31] S. Mallat, and S. Zhong, "Characterization of Signals from multiscale edges," *IEEE Transactions on Pattern Analysis and Machine Intelligence*, vol. 14, no. 7, pp. 710-732, 1992.

[32] Y. Meyer, *Wavelets Algorithms and Applications*, SIAM Publish, Philadelphia 1993.

[33] M. Nagao and T. Matsuyama, "Edge preserving smoothing," *Computer Graphics and Image Processing*, vol. 9, no. 4, pp. 394-407, 1979.

[34] K. Ramchandran, M. Vetterli, "Best wavelet packet bases in a rate-distortion sense," *IEEE Transactions on Image Processing*, Vol.2, No.2, pp.160-175, April 1993.

[35] K. Ramchandran, Z. Xiong, K. Asai and M. Vetterli, "Adaptive transforms for image coding using spatially-varying wavelet

- packets,” *IEEE Transactions on Image Processing*, vol. 5, pp. 1197-1204, July 1996.
- [36] O. Rioul, M. Vetterli, “Wavelet and signal processing,” *IEEE Signal Processing Magazine*, pp.14-38, October 1991.
- [37] N. Saito, G. Beylkin, “Multiscale representations using the auto-correlation functions of compactly supported wavelets,” *IEEE Transactions on Signal Processing*, Vol.41, no.12, pp.3584-3590, 1993.
- [38] A. Scheer, F.R.D. Velasco, and A. Rosenfield, “Some new image smoothing techniques,” *IEEE Transactions on Systems, Man and Cybernetics*, vol. 10, no. 3, pp. 153-158, 1980.
- [39] R. Schmidt, R. Nishikawa, K. Schreiber, M. Giger, K. Doi, J. Papaioannou, P. Lu, J. Stucka, G. Birkhahn, “Computer Detection of Lesions Missed by Mammography,” *Digital Mammography*, A.G. Gale et al., Editors, Elsevier Science B.V., 1994.
- [40] M. J. Shensa, “The discrete wavelet transform: wedding the a trous and Mallat algorithms”, *IEEE Transactions on Signal Processing*, vol.40, no.10, pp.2464~2482, 1992.
- [41] Z. Shi, Z. Bao, “Group-normalized processing of complex wavelet packets,” *Science in China (Serial E)*, Vol.26, No.12, 1996.
- [42] Z. Shi, Z. Bao, “Group-normalized wavelet packet signal processing”, *Wavelet Application IV, SPIE*, vol. 3078, pp.226~239, 1997.
- [43] Z. Shi, Z. Bao, “Fast image coding of interval interpolating wavelets,” *Wavelet Application IV, SPIE*, vol. 3078, pp. 240-253, 1997.
- [44] Z. Shi, G. W. Wei, D. J. Kouri, and D. K. Hoffman, “Perceptual image processing using Gauss-Lagrange distributed approximating functional wavelets,” submitted to *IEEE Signal Processing Letters*, 1998.
- [45] W. Swelden, “The lifting scheme: a custom-design construction of biorthogonal wavelets,” *Applied and Computational Harmonic Analysis*, vol.3, no.2, pp.186~200, 1996.
- [46] P. G. Tahoces, J. Correa, M. Souto, C. Gonzalez, L. Gomez, and J. J. Vidal, “Enhancement of chest and breast radiographs by automatic spatial filtering,” *IEEE Transactions on Medical Imaging*, vol. 10, no. 3, pp. 330-335, 1991.
- [47] T. D. Tran, R. Safranek, “A locally adaptive perceptual masking threshold model for image coding,” *IEEE International Conference on ASSP*, pp.1882-1885, 1996.
- [48] M. Unser, A. Aldroubi, “Polynomial splines and wavelets-a signal processing perspective,” *Wavelets-A Tutorial in Theory and Applications*, C. K. Chui (ed.), pp.91-122, Academic Press, 1992.
- [49] M. Unser, A. Adroubi, and M. Eden, “The L_2 polynomial spline pyramid,” *IEEE Transactions on Pattern Analysis and Machine Intelligence*, vol.15, no.4, pp.364-379, 1993.
- [50] P. Vaidyanathan, T.Chen, “Role of anti-causal inverse in multirate filter-banks—Part I: system-theoretic fundamentals,” *IEEE Transactions on Signal Processing*, Vol.43, No.5, pp.1090-1102, May 1995.
- [51] P. Vaidyanathan, T. Chen, “Role of anti-causal inverse in multirate filter-banks—Part II: the FIR case, factorizations, and biorthogonal lapped transforms,” *IEEE Transactions on Signal Processing*, Vol.43, No.5, pp.1103-1115, May 1995.
- [52] M. Vetterli, C. Herley, “Wavelet and filter banks: theory and design,” *IEEE Transactions on Signal Processing*, Vol. 40, No. 9, pp.2207-2232, September 1992.
- [53] J. D. Villasenor, B. Belzer, and J. Liao, “Wavelet filter evaluation for image processing,” *IEEE Transactions on Image Processing*, vol.4, no.8, pp1053-1060, 1995.
- [54] A. B. Watson, G. Y. Yang, J. A. Solomon, and J. Villasenor, “Visibility of wavelet quantization noise,” *IEEE Transactions on Image Processing*, vol. 6, pp. 1164-1175, 1997.
- [55] G. W. Wei, D. S. Zhang, D. J. Kouri, and D. K. Hoffman, “Lagrange distributed approximating Functionals,” *Physical Review Letters*, Vol. 79, No.5, pp. 775~779, 1997.
- [56] G. W. Wei, D. J. Kouri, and D. K. Hoffman, “Wavelets and distributed approximating functionals,” submitted to *Physical Review Letters*, 1998.
- [57] X. -G. Xia and Z. Zhang, On sampling theorem, wavelets and wavelet transforms, *IEEE Transactions on Signal Processing*, Special Issue on Wavelets and Signal Processing, Dec. 1993.
- [58] Z. Xiong, K. Ramchandran and M. T. Orchard, “Space-frequency Quantization for Wavelet Image Coding,” *IEEE Transactions on Image Processing*, vol. 6, pp. 677-693, May 1997.
- [59] <http://s20c.smb.man.ac.uk/services/MIAS/MIAScom.html>.